ELSEVIER

22 November 1999

PHYSICS LETTERS A

Physics Letters A 263 (1999) 70–77

www.elsevier.nl/locate/physleta

A new model of periodic precipitation incorporating nucleation, growth and ripening

Maurice Chacron, Ivan L'Heureux *

Ottawa-Carleton Institute for Physics, Department of Physics, University of Ottawa, Ottawa, Ontario, Canada K1N 6N5

Received 27 May 1997; received in revised form 28 September 1999; accepted 28 September 1999
Communicated by C.R. Doering

Abstract

We present and solve a one-dimensional model of periodic precipitation which includes nucleation, growth and ripening processes. This model thus generalizes two important models: the prenucleation-based model of Dee and the postnucleation competitive growth model (CGM) of Feeney et al. By tuning a simple phenomenological parameter, our model smoothly bridges the gap between a nucleation-growth dominated regime and one where ripening is active. © 1999 Published by Elsevier Science B.V. All rights reserved.

PACS: 36.40.Sx; 47.54.+r; 81.10.Aj
Keywords: Periodic precipitation; Liesegang bands; Competitive growth model; Prenucleation model; Postnucleation model

1. Introduction

Spatially periodic precipitation phenomena have generated much interest [1–3] ever since their first investigation by Liesegang at the end of last century. In a typical Liesegang experiment, a salt solution diffuses through an aqueous gel and reacts with another salt. According to the system geometry, the product then precipitates by forming a series of concentric rings or bands parallel to the diffusion front. Liesegang band formation have also been applied to explain various spatial patterns observed in geological systems [4–7]. The presence of the gel is not necessary as Liesegang bands have been observed in water-filled capillaries or in the gas phase [8]. In many cases, the bands obey the Jablczinsky's spacing law [9]:

$$X_{n+1} = P_n X_n \tag{1}$$

and the time scaling law [10]:

$$T_n = Q_n X_n^2. \tag{2}$$

Here, X_n, T_n denote the position and time of formation of the nth band, and P_n, Q_n tend to constants as n increases.

Models for periodic precipitation can be classified in two broad categories.

(a) In prenucleation models [11–15], a feedback mechanism exists between the nucleation kinetics and diffusional transport. Nucleation of the precipitate particles takes place when a saturation threshold is reached. Since the process is diffusion-limited,

* Corresponding author. Tel.: +1-613-562-5800/6770; fax: +1-613-562-5190; e-mail: ilheureu@physics.uottawa.ca

PII: S0375-9601(99)00709-4

precipitation results in local depletion of reactant concentration and the nucleation process is stopped. As the reaction front moves further away, a new saturation threshold is eventually reached, nucleation of precipitate is triggered and a new band is formed. The cycle repeats itself in this fashion. The models in Refs. [12–15] are based on the classical atomistic theory of nucleation. Other simpler models [3,16–19] use diffusional transport coupled with a phenomenological macroscopic expression for the saturation threshold. Cellular automata reduction of such models are also available [20]. Although the models of Refs. [14,15] incorporate growth kinetics, they are considered [21] pre-nucleation models, since the nucleation phase is essential in determining the basic features of the resulting precipitation pattern. Pre-nucleation models generate bands which are consistent with the scaling laws but do not explain other often observed features, such as pattern formation in absence of an initial concentration gradient, the time-evolution of the bands and the existence of revert spacing or other irregular patterns.

(b) In postnucleation models [4,22,23], a feedback between growth, diffusion and surface tension effects generates the pattern through a variant of the Lifshitz–Slyozov instability [24]. Here, the bands evolve through ripening after the nucleation phase is over. Homogeneous concentration profiles are unstable in such systems. Consider for example a small localized increase in particle size. This generates a local depletion of reactant. Diffusive transport then results in a net mass current towards the perturbation which increases its size. As the solution component precipitates, the particle in the zone adjacent to the perturbation will start to dissolve, thus generating an enhancement in the local concentration. This causes a net mass flux further away from the initial perturbation and growth of particle size there. The model has thus the potential to generate a succession of bands characterized by an oscillation in the particle size.

Except for some general comments in Ref. [19], a model that generalizes the two previous classes of models and reduces to them in the appropriate limits is not available. It is the purpose of this paper to present and solve such a model, in which nucleation, growth and ripening processes are present. We will specifically generalize Dee's prenucleation model [14] and the postnucleation competitive growth model (CGM) of Ref. [23]. We find that bridging the gap between a nucleation-growth dominated regime and one where ripening is important can be achieved by tuning a phenomenological parameter Δ, which characterizes the thickness of the Gibbs surface of a precipitate particle (which in turn is of the order of the critical nucleation radius). In contrast to what is assumed in many applications of the CGM, our model indicates that the number density of precipitate particles is not uniform.

2. The model

We consider a one-dimensional finite reactor of length ℓ along the spatial dimension x. Initially, the aqueous solution A (e.g., HCl) occupies the space $x < 0$ with a uniform concentration A_0, whereas the solution B (e.g., $AgNO_3$) is localized in the reactor $0 < x < \ell$ with a uniform concentration B_0. At $x = 0$, A and B react to form the product C in solution (e.g., AgCl), which can then precipitate. If $A_0 \gg B_0$, the reaction front propagates in the $x > 0$ direction. Let a, b and c be the concentration (moles per unit volume) of the reactants A and B and of the product C, respectively. Let D_1, D_2 and D_3 denote the diffusion constant of A, B and C, respectively and k the reaction rate coefficient for the reaction A + B $\rightarrow$ C, considered irreversible. Then, the following diffusion-reaction equations describe the concentrations dynamics:

$$\frac{\partial a}{\partial t} = D_1 \frac{\partial^2 a}{\partial x^2} - kab,$$

$$\frac{\partial b}{\partial t} = D_2 \frac{\partial^2 b}{\partial x^2} - kab,$$

$$\frac{\partial c}{\partial t} = D_3 \frac{\partial^2 c}{\partial x^2} + kab - u. \qquad (3)$$

Here t is time and u is the precipitation rate, i.e., the number of moles of C precipitated per unit volume per unit time.

In the spirit of the classical nucleation mechanism [25], we assume that the precipitate particles are spherical and immobile. Let $J(x,t)$ be the nucleation rate at position x and time t, $r(x,t,t')$ be the radius of a precipitate particle at time t, given that it was nucleated at time t', and let v denote the molar

volume of precipitate. Then, the molar concentration of precipitate is given by [14]:

$$f = (4\pi/3v)\int_0^t J(x,t')\,r^3(x,t,t')\,\mathrm{d}t'. \tag{4}$$

The precipitation rate is thus:

$$u = \frac{\partial f}{\partial t} = (4\pi/3v)\,J(x,t)\,r_n^3(x,t) + (4\pi/v) \times \int_0^t J(x,t')\,r^2(x,t,t')\,\frac{\partial r}{\partial t}(x,t,t')\,\mathrm{d}t'. \tag{5}$$

The first term on the right hand side of Eq. (5) represents the contribution due to the instantaneous nucleation process, $r(x,t,t)$ being the radius of the critical particle $r_n(x,t)$. The second term represents the growth of particles which nucleated in the past. We introduce the supersaturation s through:

$$s \equiv (N_0 c - C_0)/C_0 \tag{6}$$

where C_0 is the concentration (in molecules per unit volume) of the product C in equilibrium with precipitate particles of large radius and N_0 is Avogadro's number. Using classical nucleation theory, Dee [14] obtained

$$J = J_c F(s), \qquad r_n = wg(s) \tag{7}$$

where

$$F(s) \equiv \begin{cases} (1+s)^2 \exp\left(-\left[\beta g(s)\right]^2\right), & s \geq 0 \\ 0, & s < 0 \end{cases}$$

$$g(s) \equiv 1/\ln(1+s). \tag{8}$$

A similar expression for the precipitation rate is used in Ref. [15]. In these relations, the capillary length w is [22]

$$w = \frac{2v\sigma}{pN_0 k_B T} \tag{9}$$

where σ is the surface tension (assumed independent of the particle radius here), p is a stoichiometric coefficient (equal to 2 in our case), T is the temperature and k_B is Boltzmann's constant. The constants J_c and β are

$$J_c = 4\pi D_3 w^2 C_0^2/d, \qquad \beta = \left(\frac{4\pi\sigma w^2}{3k_B T}\right)^{1/2} \tag{10}$$

where d is a typical molecular size (taken as twice the diameter of the C molecule). Note that our definitnion of J_c is different from the one reported by Dee.

We now generalize this nucleation mechanism by including growth and ripening dynamics in the model. This is accomplished through a nonlinear coupling in the particle growth between the particle radius and the supersaturation, as in post-nucleation models. Although other growth laws could also be considered [15], we take the growth as interface-controlled. One has:

$$\frac{\partial r}{\partial t} = G\left[\frac{N_0 c - C_{eq}(r)}{C_0}\right] \tag{11}$$

where G is a kinetic coefficient and the Gibbs–Thomson relation:

$$C_{eq}(r) = C_0 \exp\left[w\psi(r)/r\right] \tag{12}$$

gives the molecular concentration of the product C in equilibrium with a precipitate particle of radius r. The dimensionless function $\psi(r)$ expresses the radius dependence of the surface tension, which has an important effect on the growth of particles of small radius, but is neglected in the nucleation term (Eq. (8)). Koenig [26] has derived a thermodynamically-based expression for this function:

$$\psi(r) = \exp\left[-\int_0^{\delta/r} \mathrm{d}x \frac{2\left(1+x+x^2/3\right)}{1+2x\left(1+x+x^2/3\right)}\right] \tag{13}$$

where $\delta \approx O(w)$ is a parameter characterizing the thickness of the Gibbs surface.

For computational purposes, it is convenient to approximate ψ by a rational function having the correct asymptotic behavior for large and small r. One finds to a good approximation (with a maximum relative error of 0.8%):

$$\psi(r) \cong \frac{r^2 + \delta r}{r^2 + 3\delta r + \delta^2/q} \tag{14}$$

with $q = 0.304359$. Our expression for the equilibrium concentration is new and different from the one used in the CGM.

Following Le Van and Ross [15], it is convenient to transform the integro-differential Eq. (5) to a set of coupled differential equations by defining the

average surface of the precipitate particles per unit volume Σ:

$$\Sigma \equiv 4\pi \int_0^t J(x,t,t')\, r^2(x,t,t')\, \mathrm{d}t', \tag{15}$$

the average radius of the particles per unit volume ρ:

$$\rho \equiv \int_0^t J(x,t,t')\, r(x,t,t')\, \mathrm{d}t' \tag{16}$$

and the average particle number density N:

$$N \equiv \int_0^t J(x,t,t')\, \mathrm{d}t'. \tag{17}$$

We nondimensionalize the variables according to:

$$t = \frac{w}{G} t^*, \quad x = (D_1 w/G)^{1/2} x^*, \quad a = A_0 a^*,$$

$$b = A_0 b^*, \quad \Sigma = \frac{\upsilon C_0}{N_0 w} \Sigma^*, \quad \rho = \frac{\upsilon C_0}{4\pi N_0 w^2} \rho^*,$$

$$N = \frac{\upsilon C_0}{4\pi N_0 w^3} N^*, \quad r = w r^*, \tag{18}$$

and we introduce the six dimensionless parameters:

$$K \equiv k A_0 w/G, \quad K' \equiv K A_0 N_0 / C_0,$$

$$D \equiv D_2/D_1, \quad D' \equiv D_3/D_1,$$

$$\alpha \equiv 4\pi J_c w^4 N_0 / G \upsilon C_0, \quad \Delta \equiv \delta/w \tag{19}$$

together with the dimensionless system size $L = (G/D_1 w)^{1/2}\, \ell$. In terms of dimensionless variables, we thus obtain the following generalized set of seven coupled nonlinear differential equations (dropping the $*$):

$$\frac{\partial a}{\partial t} = \frac{\partial^2 a}{\partial x^2} - Kab \tag{20a}$$

$$\frac{\partial b}{\partial t} = D \frac{\partial^2 b}{\partial x^2} - Kab \tag{20b}$$

$$\frac{\partial s}{\partial t} = D' \frac{\partial^2 a}{\partial x^2} + K' ab - (1 + s - \mathrm{e}^{\psi/r})\, \Sigma - \frac{\alpha}{3} g^3(s) F(s) \tag{20c}$$

$$\frac{\partial \Sigma}{\partial t} = \alpha g^2(s) F(s) + 2(1 + s - \mathrm{e}^{\psi/r})\, \rho \tag{20d}$$

$$\frac{\partial \rho}{\partial t} = \alpha g(s) F(s) + (1 + s - \mathrm{e}^{\psi/r})\, N \tag{20e}$$

$$\frac{\partial N}{\partial t} = \alpha F(s) \tag{20f}$$

$$\frac{\partial r}{\partial t} = 1 + s - \mathrm{e}^{\psi/r}. \tag{20g}$$

ψ is as in Eq. (14) with Δ substituting δ. Dee's prenucleation model is obtained as a special case by formally setting $\psi = 0$.

Our model also reduces to the CGM in the appropriate limit. Indeed, in the CGM, the nucleation phase is assumed terminated and only production of C by reaction, growth of the precipitate particles and ripening occur. In the CGM, the reaction-diffusion rate laws are still the same as in Eq. (3), except that the concentration of precipitate (Eq. (4)) is replaced by

$$f = \frac{4\pi N}{3\upsilon} r^3(x,t) \tag{21}$$

where N is the particle number density, assumed constant and uniform. In most applications of the CGM, N acts as a simple external parameter.

It is easily seen that, if the nucleation rate decays on a time short compared to the growth and ripening time scales of interest, and if we neglect the spatial dependence of J, then we have approximately from Eqs. (4) and (21):

$$N \cong \int_0^\infty J(t')\, \mathrm{d}t' \tag{22}$$

in agreement with Eq. (17). With N constant in time, the coefficient $\alpha F(s)$ must be set equal to zero for consistency with our model Eq. (20f). Also, one finds by integration of Eqs. (20d) and (20e) that $\Sigma = N r^2$. Scaling the variables a, b, r, t, x and N as in Eq. (18), the supersaturation evolution Eq. (20c) becomes:

$$\frac{\partial s}{\partial t} = D' \frac{\partial^2 a}{\partial x^2} + K' ab - (1 + s - \mathrm{e}^{\psi/r})\, N r^2. \tag{23}$$

This is equivalent to using Eq. (21) in Eq. (5), as in the CGM. Thus, the dynamics of the post-nucleation CGM constitutes a special case of our generalized model (Eqs. (20a), (20b), (20c), (20d), (20e) and (20f)) under the condition that N is constant and uniform. The numerical solution of our generalized model indeed shows that N becomes constant after a short time but is far from being spatially uniform.

3. Stability of a uniform sol

In order to see if the model allows for coarsening, it is useful to consider the dynamics of a spatially uniform sol in the absence of a source term (chemical reaction). Strictly, the system (20) with $K' = 0$ has no uniform steady state since Eqs. (20f) and (20g) have no common roots. However, for $F(s)$ small, N is almost constant during the times of interest. To find this uniform 'pseudo-steady state', we integrate Eq. (20c) and, with the use of Eq. (20g), we get:

$$s + N\frac{r^3}{3} = H \tag{24}$$

where H is a constant of the motion. Combining with Eq. (20g), we see that the pseudo-steady state is given by the roots of

$$e^{\psi/r} + N\frac{r^3}{3} = H + 1. \tag{25}$$

Depending on the value of H, there can be two, one or no steady-states. The linear stability of the steady state $(s_s,\ r_s)$, if it exists, can be investigated by linearizing the system about $(s_s,\ r_s)$. We assume perturbations of the form,

$$s = s_s + \varepsilon_1 \exp(ikx + \omega t),$$
$$r = r_s + \varepsilon_2 \exp(ikx + \omega t) \tag{26}$$

where $\varepsilon_{1,2}$ are small amplitudes, k is a wave-vector and ω is an eigenvalue. The solution for ω is given by

$$\omega_{\pm} = -\frac{1}{2}\left(E + D'k^2 + Nr_s^2\right) \pm \frac{1}{2}\sqrt{\left(E + D'k^2 + Nr_s^2\right)^2 - 4D'Ek^2} \tag{27}$$

where $E \equiv (de^{\psi r}/dr)|_{r_s}$. The dispersion relations $\omega_{\pm}(k)$ are schematized in Fig. 1(a) and Fig. 1(b) for

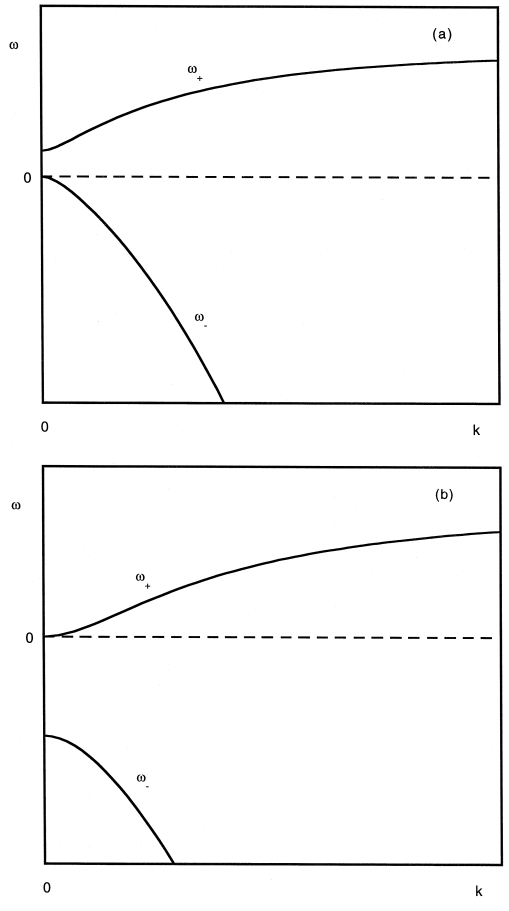

Fig. 1. Schematic representation of the dispersion curves $\omega(k)$ of Eq. (27) describing the linear stability of the uniform pseudo-steady state for the system (20): (a) $E + Nr_s^2 < 0$; and (b) $E + Nr_s^2 > 0$.

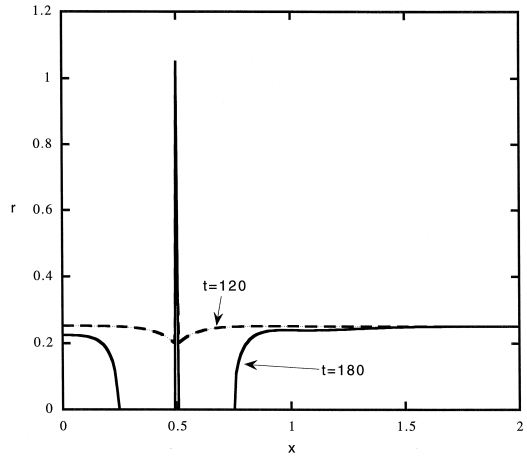

Fig. 2. Time evolution of an uniform initial condition in the absence of reaction exhibiting coarsening for $\Delta = 0.16$. The initial condition was chosen as $r = 0.25$, $s = e^{\psi/r} - 1$, $N = 1.0$, $\Sigma = Nr^2$, $\rho = Nr$. A small perturbation of amplitude 10^{-3} was applied on r at $t = 0$ and at $x = 0.5$. This perturbation resulted in a local increase of $r(0.5,t)$ and a smooth decrease (eventually to zero) in the neighborhood of the initial perturbation.

the cases where $E + Nr_s^2 < 0$ or > 0, respectively. In the first case, the steady-state is unstable to homogeneous ($k = 0$) perturbations, whereas it is stable to homogeneous perturbations in the second case. However, in both situations, the steady state is unstable to spatially-dependent perturbations ($k \neq 0$). Moreover, the maximum perturbation growth rate occurs for large k. No finite length-scale is selected by the instability, at least at this linear level of description. Thus, the system has a tendency to coarsen. These findings are analogous to the ones for the CGM.

Fig. 2 illustrates the numerical solution of the full model (Eqs. (20a), (20b), (20c), (20d), (20e) and (20f)) for an initial condition corresponding to the pseudo-steady state solution with $r_s = 0.25$ superposed to a small local perturbation at $x = 0.5$. This situation corresponds to the case of Fig. 1(a). The value of the radius tends to increase at the position of the perturbation and to decrease eventually to zero in the neighborhood of the initial perturbation.

4. Results and discussion

The initial conditions are: $a(x = 0,0) = 1$, $a(x \neq 0,0) = 0$, $b(x,0) = B_0/A_0$, $s(x,0) = -1$, $\Sigma(x,0) = \rho(x,0) = N(x,0) = r(x,0) = 0$, i.e., no precipitate exists at $t = 0$. The system dimensionless size $L = 100$ is chosen large enough with the following boundary conditions: $a(0,t) = 1$, $a(L,t) = 0$, $b(L,t) = B_0/A_0$ and a zero flux condition at the origin for the components B and C: $\partial b\ (0,t)/\partial x = \partial s(0,t)/\partial x = 0$. According to [27,28], the parameters $A_0 - B_0$ and C_0 are important parameters that characterizes the type of precipitation pattern obtained. A complete analysis of our model in terms of these parameters is outside the scope of this work. Instead, we will fix the value of these parameters and vary the phenomenological parameter Δ.

We have solved the set of parabolic partial differential Eqs. (20a), (20b), (20c), (20d), (20e) and (20f) by a non-iterative Crank–Nicholson method, with forward projection on the nonlinear terms [29]. The scheme was stable and convergent. We used dimensionless discrete time and space steps of 0.001 and 0.1, respectively. The parameter values are given by: $A_0 = 10^{-5}$ mol cm^{-3}; $B_0 = 10^{-6}$ mol cm^{-3}; $C_0 = 7.48 \times 10^{15}$ cm^{-3}; $k = 10^5$ mol^{-1} s^{-1}; $D_1 = D_2 = D_3 = 10^{-5}$ cm^2 s^{-1}; $G = 10^{-7}$ cm/s; $\sigma = 170$ erg cm^{-2}; $p = 2$; $w = 10^{-7}$ cm; $T = 300$ K; $d = 8.7 \times 10^{-8}$ cm; and $v = 25.29$ cm^3 mol.$^{-1}$. These values are typical of the system

$$AgNO_3 + HCl \rightarrow AgCl + \text{inactive products}$$

and, except for B_0, were taken from Ref. [14].

Fig. 3 illustrates the scaled precipitate molar concentration fN_0/C_0 (Eq. (3)) and the scaled radius r

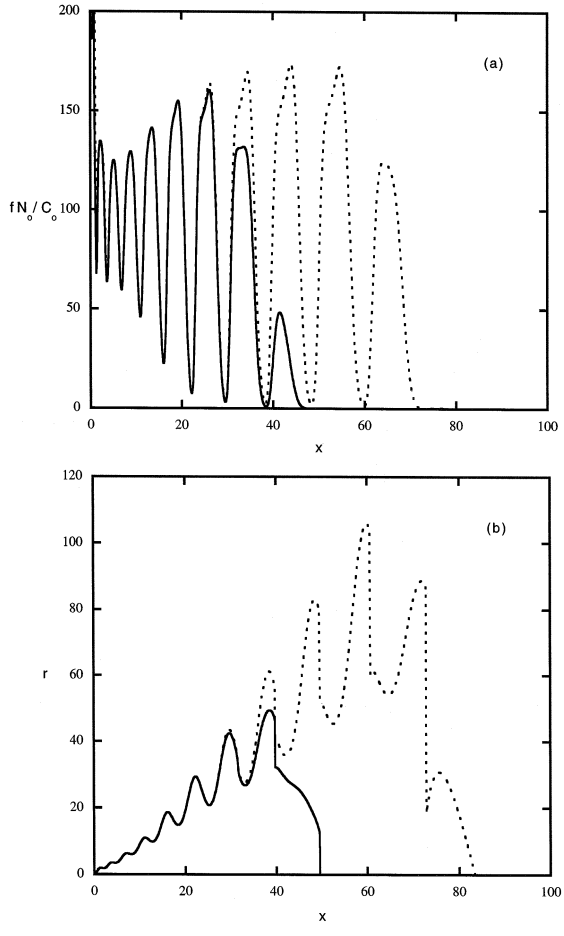

Fig. 3. (a) Scaled molar concentration of precipitate fN_0/C_0 as a function of scaled position for $\Delta = 0.16$ and for two different scaled times: $t = 300$ (continuous line) and $t = 900$ (dotted line); and (b) scaled particle radius r for the same parameter values. One dimensionless unit in x and t corresponds to 3.16×10^{-3} cm and 1 s, respectively. The scale of f is in 1.24×10^{-8} mol cm^{-3}, whereas one dimensionless unit of r corresponds to 10^{-7} cm.

as a function of the scaled distance for two different times. The value $\Delta = 0.16$ was chosen, but the time evolution turns out to be very nearly independent of Δ, as long as $\Delta \geq 0.156$. Thus, the solution exhibits the formation of precipitate bands. The density function is similar to the one obtained by Dee [14] and it is easy to verify that our precipitation pattern is consistent with the spacing and time laws of Eqs. (1) and (2). Note that the position for which the radius is a relative minimum corresponds to a maximum in the concentration, in accordance with the fact that many nuclei of small radius are nucleated. In fact, in the limit of large Δ, the ripening factor $\psi(r)/r$ is negligible for all values of r and Dee's prenucleation model is recovered.

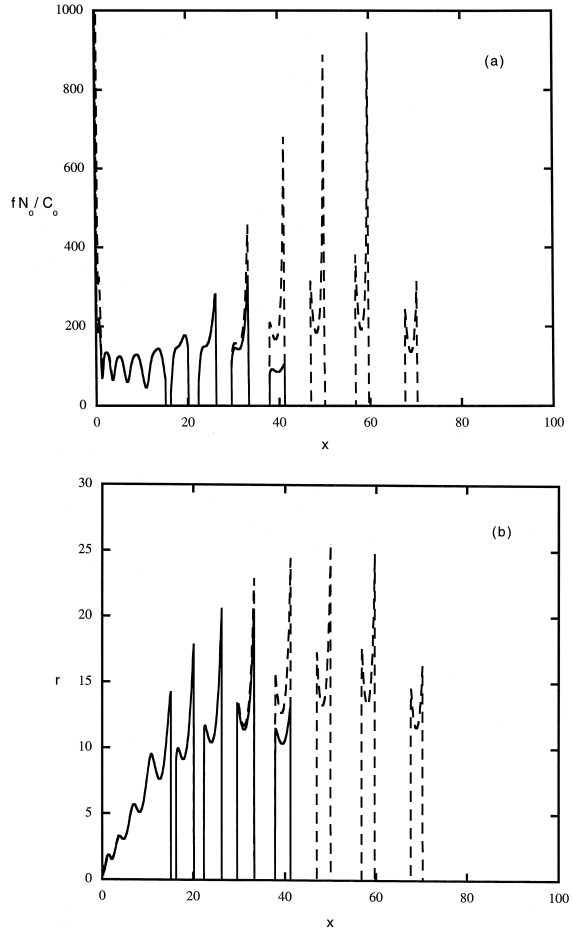

Fig. 4. Same as Fig. 3 with $\Delta = 0.136$ for $t = 300$ (continuous line) and $t = 900$ (dashed line).

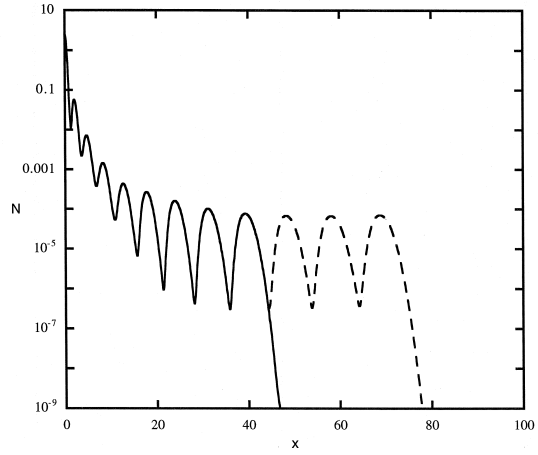

Fig. 5. Scaled particle number density for a scaled time $t = 300$ (continuous line) and $t = 900$ (dashed line), and for $\Delta = 0.136$. One dimensionless unit in N corresponds to 2.5×10^{13} cm^{-3}. The density is very nearly constant in time. The times taken to reach the first four maxima (at $x = 0.0$, 2.0, 4.7 and 8.2) are 0.71, 2.65, 6.70 and 14.18, respectively.

Fig. 4 illustrates the same quantities, but using a smaller value of $\Delta(= 0.136)$. The solution is quantitatively different. For the later stages of the process and for a position larger than some threshold, the bands continue to evolve after their formation: they create a doublet (satellites). Thus, each band is eventually characterized by two narrow sub-bands of high-density aggregate, separated by a wider zone of low-density precipitate. During this phase of the process, a minimum in the radius tends to occur at the same position as a minimum in the precipitation, indicating that ripening is taking place. Another feature of the solution is to exhibit interbands regions where no precipitate exist. These characteristics are typically found in postnucleation models of periodic precipitation and are also observed in nature [4]. As the value of Δ is further decreased, the solution is similar to the case of Fig. 4 except that the doublet formation is more pronounced: the contrast between the high-density edges of the doublet and its low-density middle region is enhanced.

A CGM solution with a typical, constant and uniform value of the particle number density N, also generates doublets in the molar concentration of precipitate. However, in contrast to our model where both ripening and nucleation take place, the solution

obtained from the CGM exhibits much higher and narrower peaks in the molar concentration of precipitate than those in Fig. 4. Moreover, our results (Fig. 5) show that, whereas N is indeed nearly constant in time, it is far from uniform. A banding pattern is also reflected in the spatial dependence of N.

5. Conclusion

In this paper, we have presented a periodic precipitation model which smoothly bridges the gap between a regime where nucleation and growth are dominant and one where ripening is important by varying a simple phenomenological parameter Δ. This parameter is a by-product of our expression for the radius-dependence of the surface tension and characterizes the thickness of the Gibbs surface. For large values of Δ, the system exhibits the formation of bands of precipitate mostly via nucleation and diffusional transport as in Dee's prenucleation model. For small values of Δ, the ripening mechanism becomes important and further evolution of the bands is characterized by the formation of doublets, as in the CGM.

One basic assumption underlying the applications of the CGM is that the precipitate number density is constant, uniform and a priori known. By direct computation, we have found that, although the number density is very nearly constant, it is far from uniform. This feature and the fact that nucleation is not neglected in our model explains why our solutions are quantitatively different from those obtained in the CGM.

As in many periodic precipitation models, ours neglects fluctuations and thus constitutes a mean-field approach to the problem. A more complete analysis would require the calculation of the probability density of finding a crystal with radius between r and $r + dr$ at position x and time t. This could be achieved by using our Gibbs–Thomson relation in existing molecular theories of coarsening in periodic precipitation patterns (see for example [30,31]) or by incorporating the precipitation reactions to existing theories of phase separation combining nucleation, growth and ripening [32].

Acknowledgements

This research was supported by grants from the Natural Sciences and Engineering Research Council of Canada. I.L. acknowledges fruitful discussions with A.D. Fowler.

References

[1] R.E. Liesegang, Photogr. Archiv. 21 (1896) 221.
[2] K.H. Stern, Chem. Rev. 54 (1954) 79.
[3] H.K. Henisch, Periodic Precipitation, Pergamon Press, Oxford, 1991.
[4] A.E. Boudreau, Min. Pet. 54 (1995) 55.
[5] A.E. Boudreau, S. Afr. J. Geol. 97 (1994) 473.
[6] P. Ortoleva, Geochemical Self-Organization, Oxford University Press, New York, 1994.
[7] I. L'Heureux, A.D. Fowler, in: B. Jamtveit, P. Meakin (Eds.), Growth, Dissolution and Pattern Formation in Geosystems, Kluwer Academic Publishers, Amsterdam, 1999.
[8] A. Büki, E. Kárpáti-Smidróczki, M. Zrínyi, Physica A 220 (1995) 357.
[9] K. Jablczynski, Bull. Soc. Chim. France 33 (1923) 1592.
[10] H.W. Morce, G.W. Pierce, Physik. Chem. 45 (1903) 589.
[11] W. Ostwald, Lehrbuch der Allgemeinem Chemie, Engelman, Leipzig, 1897.
[12] S. Prager, J. Chem. Phys. 25 (1956) 279.
[13] D.A. Smith, J. Chem. Phys. 81 (1984) 3102.
[14] G.T. Dee, Phys. Rev. Lett. 57 (1986) 275.
[15] M.E. Le Van, J. Ross, J. Phys. Chem. 91 (1987) 6300.
[16] Y. Brechet, J.S. Kirkaldy, J. Chem. Phys. 90 (1989) 1499.
[17] V. Talanquer, J. Chem. Educ. 71 (1994) 58.
[18] A. Büki, E. Kárpáti-Smidróczki, M. Zrínyi, J. Chem. Phys. 103 (1995) 10387.
[19] D.S. Chernavskii, A.A. Polezhaev, S.C. Müller, Physica D 54 (1991) 160.
[20] B. Chopard, P. Luthi, Phys. Rev. Lett. 72 (1994) 1384.
[21] R. Lovett, P. Ortoleva, J. Ross, J. Chem. Phys. 69 (1978) 947.
[22] A.A. Polezhaev, S.C. Müller, Chaos 4 (1994) 631.
[23] R. Feeney, S.L. Scmidt, P. Strickholm, J. Chadam, P. Ortoleva, J. Chem. Phys. 78 (1983) 1293.
[24] I.M. Lifshitz, V.V. Slyozov, J. Phys. Chem. Solids 19 (1961) 35.
[25] I.V. Markov, Crystal Growth for Beginners, World Scientific, Singapore, 1996.
[26] F.O. Koenig, J. Chem. Phys. 18 (1950) 449.
[27] S.C. Müller, S. Kai, J. Ross, J. Phys. Chem. 86 (1982) 4078.
[28] S. Kai, S.C. Müller, J. Ross, J. Phys. Chem. 87 (1983) 806.
[29] D.U. von Rosenberg, Methods for the Numerical Solution of Partial Differential Equations, Elsevier, New York, 1969.
[30] G. Venzl, Phys. Rev. A 31 (1985) 3431.
[31] G. Venzl, J. Chem. Phys. 85 (1986) 1996.
[32] C. Sagui, M. Grant, Phys. Rev. E 59 (1999) 4175.